Solid-State Lasers

The use of lasers played a crucial role for the evolvement and practical implementation of nonlinear optics. In this Chapter, an overview of the governing relations in laser theory and some important equations is given. In the last part, results from a numerical simulation of a passively Q-switched quasi-three level laser are presented. These simulations were conducted during the development of the UV laser source described in Chapter 6, as a means to optimise the fundamental light source.

2.1 Basic theory

A laser is based on the concept of stimulated emission of radiation, where an electron is stimulated by a photon to give up its energy and decay to a lower energy level. In this process, another photon is created having exactly the same characteristics as the first photon in terms of frequency, polarisation, phase and propagation direction. The condition for this to happen is that the energy of the incoming photon matches the energy level difference between the higher and lower energy states, or

$$E_p = h\upsilon \approx E_j - E_i, \tag{2.1}$$

where $E_j > E_i$, ν is the frequency of the incoming photon and h is Planck's constant. This expression states that the energy of the incoming photon does not have to exactly equal the energy difference between the two electron states. The probability function for a photon to interact with a atom is not given by Dirac's delta function centred at ν, but is broadened with respect to the frequency into a lineshape function $g(\nu)$. This lineshape function can have different appearances depending on the type of broadening that is present in the specific atomic system. There exist mainly two types of broadening, homogeneous and inhomogeneous broadening. The first type describes a system where all atoms are indistinguishable and have the same transition energy and central frequency. Here, the overall lineshape of the absorption cross section is identical with the lineshape of the single-atom cross-section. In this case, the emission of a photon at a certain frequency reduces the subsequent average probability homogeneously over the linewidth. In for example Nd:YAG, the main homogeneous broadening mechanism is thermal broadening, where the thermal vibrations of the lattice surrounding the active ions influences the atomic transition. Inhomogeneous broadening on the other hand describes a system where the atoms are distinguishable, and the emission of a photon will reduce the subsequent average probability inhomogeneously over the linewidth. The overall response of a collection of atoms to an applied signal is broadened, due to displaced centre frequencies of the individual atoms. For solid-state lasers, crystal inhomogeneities can be a cause for inhomogeneous broadening. This may lead to so-called spectral hole-burning, where the emission around a certain frequency is temporarily obstructed because of reduction of the gain at that particular frequency (a "hole" is burned in the gain curve).

Not only the stimulated emission process is possible in the photon-electron interaction between two energy states E_i and E_j, but also the two processes absorption and spontaneous emission. Absorption is essentially the inversion of stimulated emission, where an atom with an electron in the lower energy state absorbs a photon of energy E_p and is thus excited to the higher energy state. Whereas stimulated emission involves radiation of a photon that is an exact copy of the incoming photon, spontaneous emission is a process where an electron is spontaneously de-excited into the lower energy state, thereby emitting a photon of random phase and propagation direction. Its energy (and thus its frequency distribution) is described by the lineshape function $g(\nu)$.

In thermal equilibrium, the population density N_j (population number per volume) of the state of higher energy is lower than that of the lower energy state according to Boltzmann statistics, but if the population densities are inverted, this will result in an exponential decay of the population density N_j into the lower level E_i. This decay will governed by a timeconstant τ_j, called the spontaneous emission lifetime.

2.2 Intensity gain and absorption

By considering a thin slab of thickness *dz* submitted to an applied optical signal of intensity *I*, it is possible to derive expressions for gain and absorption as function of the population densities. A schematic picture of the energy level system for the media can be seen in Fig. 2.1. It is assumed that the atoms in the slab have an average absorption cross-section σ_{ij}, which gives the probability for an atom to be excited to the higher energy state E_j. Likewise, there is a corresponding probability for the atom to relax into the lower energy state E_i upon emitting a photon which is related to the stimulated emission cross section σ_{ji}. Then, the power emitted or absorbed by an individual atom in the slab is given by $\sigma \cdot I$. Taking all atoms of the slab into account, the total intensity absorbed in the length element *dz* is consequently $N_i \sigma_{ij} dz \cdot I$.

Similarly, the total emitted intensity is $N_j \sigma_{ji} dz \cdot I$. The net difference is thus[4-6]

$$dI = \left(N_j \sigma_{ji} - N_i \sigma_{ij}\right) I dz \tag{2.2}$$

It should be noted that the absorption cross section and the stimulated emission cross sections are related through the expression $\sigma_{ji} = \sigma_{ij} g_i / g_j$ [5,6], where the g_i and g_j are the degeneracy factors of the states E_i and E_j, respectively. The light beam of initial intensity *I* will thus experience a net gain or decay depending on the sign of $N_j \sigma_{ji} - N_i \sigma_{ij}$, thereby implying that N_j has to be larger than $N_i g_j / g_i$ in order for the optical signal to be amplified. Rewriting the expression above gives the following differential equation

$$\frac{dI}{dz} = \sigma_{ji} \Delta N \cdot I \tag{2.3}$$

where the so-called population-inversion density is defined as $\Delta N = N_j - N_i g_j / g_i$. This equation can be easily solved according to

$$I(z) = I(0)\exp(\sigma_{ji}\Delta N \cdot z) \tag{2.4}$$

Here, the gain coefficient is defined as $g = \sigma_{ji}\Delta N$, implying that if $N_j > N_i g_j / g_i$, the optical signal will grow exponentially as it traverses the slab. On the other hand, if there is no population inversion (i.e. $\Delta N < 0$), there will be a net absorption of the optical signal in the medium. The corresponding absorption coefficient is then defined as

$$\alpha = \left(\frac{g_j}{g_i} N_i - N_j \right) \sigma_{ji} . \tag{2.5}$$

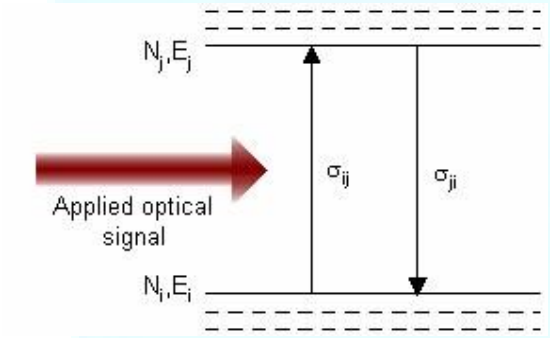

Fig. 2.1 Schematic of the energy levels with their absorption and emission crosssections.

It is important to note that population inversion can never be reached in a two-level system. This is since the probability for absorbing a photon is exactly equal to the probability of emitting a photon, once $N_j = N_i g_j / g_i$. In other words, the absorption becomes saturated and the additional absorption required for population inversion will not occur. Thus, the gain required for lasing action is achieved in multi-level systems. A typical example is the fourlevel laser system, where an energy state at a higher level than E_j, termed E_k, together with the ground state with the energy E_0 are taking part in the stimulated emission process. Here, the electrons in the ground state are excited, often by means of optical pumping, to the highest energy state with energy E_k, and from there it rapidly decays to E_j through non-radiative relaxation. In order for the process to be efficient, the time-scale of this decay must be much shorter than the spontaneous emission life-time of the energy state E_j. If the population of the lower energy state E_i is negligible at thermal equilibrium, population inversion between E_j and E_i is easily reached and stimulated emission takes place between the upper laser level E_j and the lower laser level E_i. In addition, fast relaxation from E_i to E_0 is also desirable for reaching population inversion between the laser levels. Nevertheless,

other laser systems are also possible, such as the three-level laser system where the lower laser level coincides with the ground-state E_0. In materials exhibiting Stark splitting of the energy states, i.e. when sublevels are present within the different energy levels, the lower laser level can be thermally populated if it lies close enough to the ground-state level. In this case, the system is called a quasi-three level laser system. In the following sections, the latter kind of laser system will be modelled using the so-called rate equations.

2.3 Rate equations

The modelling of laser systems are often expressed through the rate equations. As an example, the 946 nm laser transition of Nd:YAG is considered. This transition takes place between the lowest Stark level of the energy state $^4F_{3/2}$ and the highest Stark level of the energy state $^4I_{9/2}$, as seen in Fig. 2.2. Thus, the lower laser level is a sublevel of the ground state level.

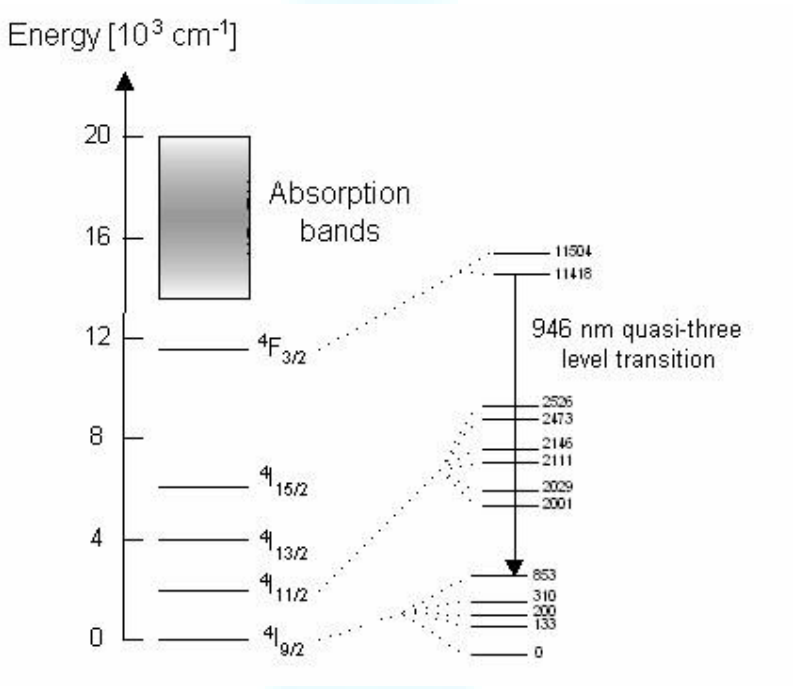

Fig. 2.2 The energy diagram for Nd^{3+} in the YAG host. For clarity, only the Stark sublevels of the two lowest energy levels and the upper laser level are shown.

This is a quasi three-level system where the Nd^{3+} ions are excited from the ground state into the absorption level 3 and then very rapidly decay via multiphonon relaxations down to the metastable upper laser level 2. After the laser transition, the ions relax from the upper Stark level of the energy state $^4I_{9/2}$ to the lowest level within the same manifold. A simplified scheme of the energy levels with their corresponding population densities and life-times is shown in Fig. 2.3. Here, the ground state and upper laser level population densities are N_1 and N_2, respectively and the population density of the absorption level is termed N_3. The doping concentration or the total population density is termed N_0 and for the laser system described here, N_3 is so small that $N_0 \approx N_1 + N_2$.

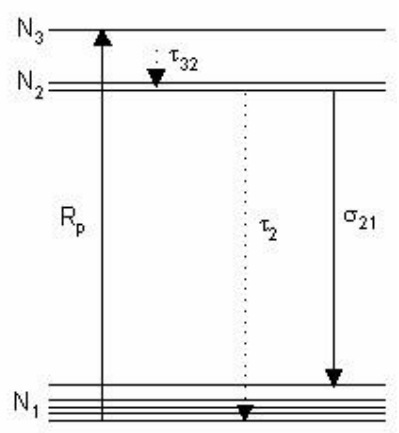

Fig. 2.3 The energy diagram for a quasi-three-level laser system.

The excitation of the ions at the ground state into the absorption level is typically achieved employing optical pumping. In this work, laser diodes have been used in an end-pumping configuration. All of the pump power of the laser diode is not absorbed by the laser crystal, and the fraction of the incident power that is absorbed is called the absorption efficiency, given by $\eta_a = 1 - \exp(-\alpha l_{cr})$ as can be deduced from Eq. 2.4 and Eq. 2.5, where l_{cr} is the length of the crystal and α is the absorption coefficient given by $\alpha = \sigma_p N_0$. It should be noted that in the latter expression pump saturation has been neglected, and is thus an approximation. In addition, it has been assumed that the pump beam makes a single-pass through the material. Also, an effective absorption cross section σ_p have been used for the transition from the ground-state level to the absorption band. The pumping process to the absorption band is described by the pump rate density R_p given by

$$R_p(x,y,z) = \frac{\eta_a \eta_p \lambda_p P^P r_p(x,y,z)}{hc_0} \quad (2.6)$$

where η_p is the quantum efficiency of the pumping process, λ_p is the centre wavelength of the pump source, c_0 is the velocity of light in vacuum and P_p is the incident pump power. It should be noted that η_p can be close to unity when using a pump with a narrow bandwidth (e.g. a laser diode), whereas for flash lamp pumping, it can be significantly reduced. The function r_p is the normalised spatial distribution of the pump beam over the laser crystal. This function is usually considered to be Gaussian, but for simplicity it is here assumed to have a top-hat shape. Also neglecting exponential decay of the pump power, the pump rate density can then be written as

$$R_p = \frac{\eta^p \alpha \lambda_p}{hc_0} \cdot \frac{P^p}{A_{eff}} \quad (2.7)$$

where $A_{eff} = \pi \omega_p^2 / 2$ is the effective Gauss area for a pump beam with $1/e^2$-radius ω_p. In addition, an effective pump radius can be defined as[7]

$$\bar{w}_p^2 = \frac{\int_0^{l_{cr}} w_p^2(z)\exp(-\alpha z)\,dz}{\int_0^{l_{cr}} \exp(-\alpha z)\,dz} \tag{2.8}$$

where l_{cr} is the length of the laser crystal and $w_p(z)$ is described as a Gaussian beam using the beam propagation factor $M^2 = 52$ for the pump source.

In order to model how the photon density builds up inside a laser, a simple cavity with two mirrors and a laser crystal with refractive index n is considered. The reflectivity of the outcoupling mirror is R, and the optical path length of the cavity is l_c^*. A residual round-trip loss L is assumed. If the spatial distribution of the laser mode is considered to be a uniform top-hat function instead of Gaussian, the rate equations governing the temporal dynamics of the population densities of the laser levels N_1 and N_2 as well as the photon density φ can be formulated according to [5,6]

$$\begin{aligned} \frac{dN_2}{dt} &= -\frac{dN_1}{dt} = R_p - \frac{N_2}{\tau_2} - c_0\sigma_{21}\Delta N\varphi \\ \frac{d\varphi}{dt} &= \frac{\varphi}{t_r}\left(2\sigma\Delta N l_{cr} - \delta\right) \end{aligned} \tag{2.9}$$

where $t_r = 2l_c^*/c_0$ is the round trip time in the laser cavity and $\delta = L - \ln R$ is the total round trip loss in the cavity. A so-called cavity lifetime of the photons can be defined from these two parameters, given by $t_c = t_r/\delta$. It should be noted that the population inversion density ΔN is the difference in population density between the Stark levels, which are populated according to the Boltzmann distribution at thermal equilibrium. The fraction of the total population density N_2 residing in the upper laser level is denoted f_b, so that the actual population density is $N_b = f N_{b2}$, where

$$f_b = \frac{g^b \exp\left(-\Delta E^{2b}/k_B T\right)}{Z_2} \tag{2.10}$$

Here, k_B is Boltzmann's constant, T is the temperature and

$$Z_2 = \sum_{i=1}^{m} g_i \exp\left[-\Delta E_{2i}/k_B T\right] \tag{2.11}$$

is the partition function of level 2. The energy difference between sublevel i and the lowest sublevel within the manifold is denoted ΔE_i and g_i is the degeneracy of sublevel i. Similarly, the fraction of the total population density N_1 in the lower laser level is denoted f_a and the actual population density is consequently $N_a = f N_{a1}$. Thus, the population inversion density in Eq. 2.9 is given by $\Delta N = N_b - N_a$.

Since there is a non-negligible fraction of the ground-state population density residing in the lower laser level, this gives rise to reabsorption effects, i.e. laser photons produced in the stimulated emission process are absorbed by the ions in the lower laser level which are then excited to the absorption band, instead of contributing to the laser photon amplification in the cavity. This effect is implicitly taken care of in the above formulated rate equations.

2.4 Energy-transfer upconversion

It has previously been shown[8-13] that energy-transfer upconversion (ETU) is a detrimental effect in Nd-doped lasers. This effect involves the ions residing in the upper laser level, where two nearby ions interact in an upconversion process. One ion relaxes down to a lower lying energy state and transfers its energy to the other ion, which is thereby raised (upconverted) to a higher energy state. Consequently, ETU reduces the population of the upper laser level and thus the population inversion, which in turn degrades the overall laser performance.
Here, it is considered that the decay rate via multiphonon processes from the energy states involved in the ETU process is much faster than the life-time of the upper laser level. The net effect is that only one excited ion is removed from the upper laser level by each upconversion process, since the upconverted ion will decay rapidly back to the upper laser level.
Including ETU effects in the modelling of the laser system above, modifies the rate equation for the upper laser level according to

$$\frac{dN_2}{dt} = \frac{dN_1}{dt} = R_p - \frac{N_2}{\tau_2} - c_0\sigma_{21}\Delta N\varphi - WN_2^2 \qquad (2.12)$$

where W is the so-called upconversion rate parameter which has the value $2.8\cdot10^{-22}\, m^3 s^{-1}$ for Nd:YAG[8]. The main consequences of ETU are heat generation and reduced available gain.

2.5 Passive Q-switching

In many applications, high output power is advantageous. One way of achieving high peak power lasers is by compressing the power generated in a laser cavity into short, energetic pulses. A widely used technique for realising these pulses is the so-called Q-switching technique[14]. This technique is based on the concept of modulating the losses inside the laser cavity, thereby modulating the ratio of the stored energy to the loss per cycle, i.e. the Q-value.

The modulated loss can be pictured as a shutter inside the cavity, which is either closed or open. If the shutter is closed, laser action is prevented and the population inversion can continue to build up as the laser crystal is pumped continuously. When the shutter opens, the laser will exhibit a gain that greatly exceeds the losses. The stored energy may then be released in the form of a short and intense light pulse.

A compact and practical way of Q-switching solid-state lasers is to use saturable absorbers in the laser cavity[15]. This kind of Q-switching is passive, since no external driving sources are needed. A saturable absorber consists of a material that absorbs at the laser wavelength and becomes almost transparent for a low incident light intensity, thus behaving as a variable loss in the laser cavity. As the laser medium is pumped, the energy in the cavity builds up and approaches the threshold condition despite the extra loss introduced by the absorber. A weak resonating field begins to grow in the cavity, which successively becomes strong enough to bleach the saturable absorber. The bleaching occurs when the ground-state level of the absorber is depleted. However, this bleaching can be incomplete and thus cause residual absorption losses in the saturable absorber. Another disadvantage of using saturable absorbers is timing jitter, which is connected to mechanical as well as temperature instabilities in the laser system.

In the 1 μm spectral region, Cr^{4+}:YAG is often chosen because of its large absorption cross-section and low saturable intensity at the laser wavelength. In addition, it has a high damage threshold and is photochemically and thermally stable. It also provides the possibility of a compact and simple laser cavity. The energy level system of the Cr^{4+}:YAG crystal is shown in Fig. 2.4. As Cr^{4+}-doped crystals are susceptible to excited state absorption (ESA)[16], a four-level model is used to analyse its performance as a Q-switch. Absorption of the laser wavelength takes place at the 1-3 transition as well as the ESA at the 2-4 transition and the corresponding absorption cross-sections are σ_{gs} and σ_{es}, respectively. The relaxation rate for the transitions 4-2 and 3-2 is fast, while the life-time of level 2 is $\tau_s = 4.1$ μs[17] for Cr^{4+}:YAG. Thus, only the ground level 1 and level 2 have non-negligible population densities, termed N_{s1} and N_{s2}. The total population density participating in transitions is N_{s0} and can be obtained from the following expression[17] (in accordance with Eq. 2.4)

$$T_0 = \exp\left(-N_{s0}\sigma_{gs}l_s\right) \tag{2.13}$$

where T_0 is the initial (small-signal) transmission and l_s is the thickness of the absorber crystal.

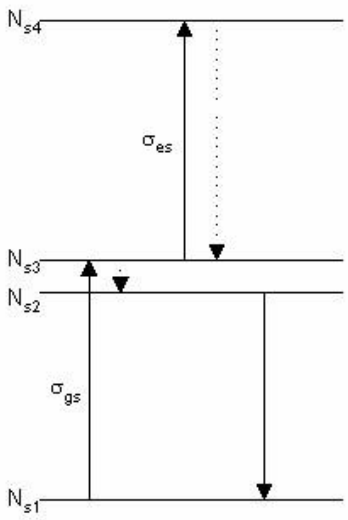

Fig. 2.4 The four-level model of the Cr^{4+}-doped saturable absorber.

To model a passively Q-switched laser, the coupled rate equations can be written as[16,18]

$$\frac{dN_b}{dt} = f R_{b\,p} - \frac{N_b}{\tau_2} - f c_{b\,0}\sigma \varphi_{21}\Delta N - W N_{b2}$$

$$\frac{dN_a}{dt} = -f_a \frac{dN_a}{dt} = -f_a R_p + \frac{f N_{a\,2}}{\tau_2} + f c_{a\,0}\sigma \varphi_{21}\Delta N + f W N_{a\,22} \qquad (2.14)$$

$$\frac{d\varphi}{dt} = \frac{\varphi}{t_r}\left(2\sigma_{21}\Delta N l_{cr} - 2\sigma_{gs} N_{s1\,s} l_{s1\,s} - 2\sigma_{es}\left(N_{s0} - N_{s1}\right) l_s - \delta\right)$$

$$\frac{dN_{s1}}{dt} = -\frac{dN_{s2}}{dt} = -c_0 \sigma \varphi_{gs} N_{s1} + \frac{\left(N_{s0} - N_{s1}\right)}{\tau_s}$$

where the temporal dynamics of the ground-state population density in the saturable absorber is governed by the last equation. In the equations above, it has been assumed that the size of the laser mode is equal in the laser crystal and in the saturable absorber so that the photon density in the same in all equations. By numerically simulating the temporal dynamics of the rate equation system above, the proper choice of initial transmission of the saturable absorber and transmission $T = 1\text{-}R$ of the output coupler can made in order to optimise the performance of the passively Q-switched laser. However, Degnan *et al*[19] extended the rate equations to include the effect of thermalization, i.e. single phonon-assisted transitions between nondegenerate Stark sublevels. Since the energy level differences in each multiplet lies within

the highest phonon energies in Nd:YAG (the highest phonon energies are in the order of 700 cm^{-1} [20]), the thermalization transitions between non-degenerate Stark sublevels within either of the two multiplets is hence probable. By introducing the so-called thermalization time-constants τ_u and τ_l for the upper and lower laser multiplets, respectively, the rate equations are modified according to

$$\frac{dN_b}{dt} = f_b R_p \left(N_b - f_b N_{b2}\right) - N_b \left(\frac{1}{\tau_u} + c_0 \sigma \varphi_{21} \Delta N + W N_{b2}\right)$$

$$\frac{dN_a}{dt} = -f_a R_p \left(N_a - f_a N_{a1}\right) + \frac{f_b N_{b2}}{\tau_l} + \frac{f_a N_{a2}}{\tau_2} + c_0 \sigma \varphi_{21} \Delta N + f_a W N_{a22} \qquad (2.15)$$

$$\frac{dN_2}{dt} = R_p - \frac{N_2}{\tau_2} - c_0 \sigma \varphi_{21} \Delta N - W N_{22}$$

$$\frac{dN_1}{dt} = -\frac{dN_2}{dt} = -R_p + \frac{N_2}{\tau_2} + c_0 \sigma \varphi_{21} \Delta N + W N_{22}$$

where the equations for the photon population density and the ground-state population density in the saturable absorber are the same as in Eq. 2.14 and have hence been omitted. Here, N_2 and N_1 refer to the total population densities in the upper and lower lasing manifold, respectively. Within their respective multiplets, the population densities in the upper and lower Stark sublevels are denoted N_b and N_a, respectively.

The total number of photons in the cavity can be calculated from the following integral

$$\frac{d\Phi}{dt} = \int_{cavity} \int \int \frac{d\varphi}{dt}\, dV \qquad (2.16)$$

and is related to the output power as $P_{out} = Th\upsilon_L \Phi t_r$ where ν_L is the laser frequency. In the simulations described in the following section, it has been used that the laser mode radius is smaller than the pump mode radius, so the integration in (2.16) is taken over the laser mode volume. Thus, the population density is given by $\varphi = \Phi V_L$, where $V_L = l_c \pi \omega_L^2$.

2.6 Q-switching performance of a quasi-three level Nd:YAG laser

The rate equations above (Eq. 2.15) can be applied to the passively Q-switched quasi-three level Nd:YAG laser described in Paper VI. The laser in question comprised a 15 mm long composite rod with a 5 mm long Nd:YAG crystal (doping level 1.1 atm%) and two undoped end-caps each 5 mm in length. The end-caps allow for a longitudinal heat flow when the crystal is heated by the pump, which reduces the thermal effects. Its diameter was 3 mm and it was directly watercooled to a temperature of 15 ˚C. A planar incoupling mirror and an outcoupling mirror with a ROC = 200 mm and transmission of 12 % were used, and the total cavity length was approximately 26 mm. A 0.5 mm thin uncoated Cr:YAG disc (employed in Brewster's angle to yield polarised laser output) with an initial transmission of 94 % was used as a saturable absorber. A fiber-coupled 808-nm diode (Limo GmbH) was used as the pump source, emitting up to 21 W from a 200 µm fibre with a NA of 0.22. For 7 W of absorbed power, the average output power was 0.94 W and the repetition frequency was 22 kHz whereas the pulse length was 16 ns as stated in Paper VI. These values correspond to a peak power of 2.9 kW and a pulse energy of 43 µJ.

In the simulations, the residual loss term was appreciated to L = 5.5 %, where additional absorption losses of the Cr:YAG crystal is taken into account. The additional absorption loss originating from water absorption is described in paper VI. Furthermore, the depolarisation loss[21] at this particular pump power is appreciated to 0.5 %. With this value of the loss factor and using that the cavity round-trip time is 0.26 ns, a cavity photon lifetime of 1.5 ns can be calculated. Thus, the pulse length is approximately 11 times longer than the cavity lifetime. The other input parameters used in the simulations were as follows: $N_0 = 1.5 \times 10^{20}$ cm^{-3} [22], n = 1.82, $\tau_2 = 230$ µs [23], $\sigma_{21} = 5.1 \times 10^{-22}$ cm^2 [24], $\tau_s = 4.1$ µs [16], $\sigma_{gs} = 4.0 \times 10^{-18}$ cm^2 [25] and $\sigma_{es} = 1.1 \times 10^{-18}$ cm^2 [25]. The absorption coefficient α was determined experimentally to about 2.48 cm^{-1}, and given that the launched pump power was 9.85 W, the fraction of the pump absorbed in the crystal is then 71 %. A laser mode radius of 109 µm and an effective pump radius of 160 µm were used in the simulations. As for the thermalization time-constants, no exact data exist in the literature. The time-constant for the upper multiplet was appreciated to 3-5 ns in the article by Degnan *et al*[19], but for the lower multiplet no data could be found in the literature. If one considers that since the energy difference ΔE between the Stark levels in the lower multiplet is larger than in the upper multiplet, and assume that the time-constants follow the energy-gap law[26] $\tau \tau^{-1} = {}_0{}^{-1} \exp(-\Delta\gamma E)$and use the slope parameter $\gamma = 5.24 \times 10^{-3}$ cm^{-1} [27], it can be deduced that the thermalization time-constant for the lower laser multiplets is approximately 11 times longer than for the upper laser multiplets. Considering that the pulse length was 16 ns, thermalization time-constants of these orders should have an impact on the performance of the laser. It was found that the numerical values got closest to the experimentally achieved results of peak power, repetition frequency and pulse length provided that thermalization time-constants of 5 ns for the upper laser level[19] and 55 ns for the lower laser level are assumed. However, the numerical simulation predicts a too short pulse length of 10 ns compared to the experimental value of 16 ns. Also the numerical values of peak power (3.09 kW), repetition frequency (30 kHz) and pulse energy (54 µJ) were too high. Nevertheless, when no thermalization effects are taken into account, i.e. Eq (2.14) is used instead of Eq. (2.15), the numerical values do not even get close to the experimental results for any values of the input parameters. In general, the Q-switching model without thermalization predicts too short pulse lengths and much too high peak powers. Using the

same input parameters as given above but neglecting thermalization would result in a pulse length of 6 ns and a peak power of 22 kW.

To see how thermalization and also upconversion effects influenced the pulse characteristics, numerical simulations were carried out with using Eq. 2.15 and Eq. 2.14, using the same input parameters and setting $W = 0$ in order to neglect upconversion. The result is presented in Fig. 2.5. The effect of the thermalization is that the pulse dynamics includes several peaks instead of just one, as in the two lower graphs of Fig. 2.5. The reason for this behaviour is nontrivial, but it can be understood that thermalization modulates the population inversion and thus the pulse dynamics through the thermalization terms in Eq. 2.15. As for the upconversion, it does not seem to influence the pulse characteristics to a greater extent when thermalization is taken into account, but it has a large effect on the peak power when thermalization is neglected, as can be seen when comparing the two lower graphs.

Although the numerical simulations can not exactly predict the experimental results, I also investigated how different transmission of the outcoupling mirror for the laser and the initial transmission of the saturable absorber would affect the laser characteristics. The results of the simulations are presented in Fig. 2.6-2.9. As expected, a lower initial transmission of the saturable absorber yields a higher peak power combined with a shorter pulse length and a lower value of the repetition frequency. However, these demands must be balanced with the risk of damage of the coatings on the crystals in the laser cavity. In addition, the reabsorption losses inherent in quasi-three level lasers impose limits on the optimum choice of initial transmission as well as the output coupler transmission.

The effective radius is also a crucial parameter when designing Q-switched lasers. In Fig. 2.10-2.13, the dependence on the effective radius of the pump beam is presented. As a lower initial transmission of the saturable absorber acts as larger round-trip loss for the Q-switched laser during population-inversion build-up, this sets demands on the size of the focused pump beam waist. As seen from Fig. 2.10, the optimum peak power occurs for a smaller effective pump beam radius when the initial transmission is lower.

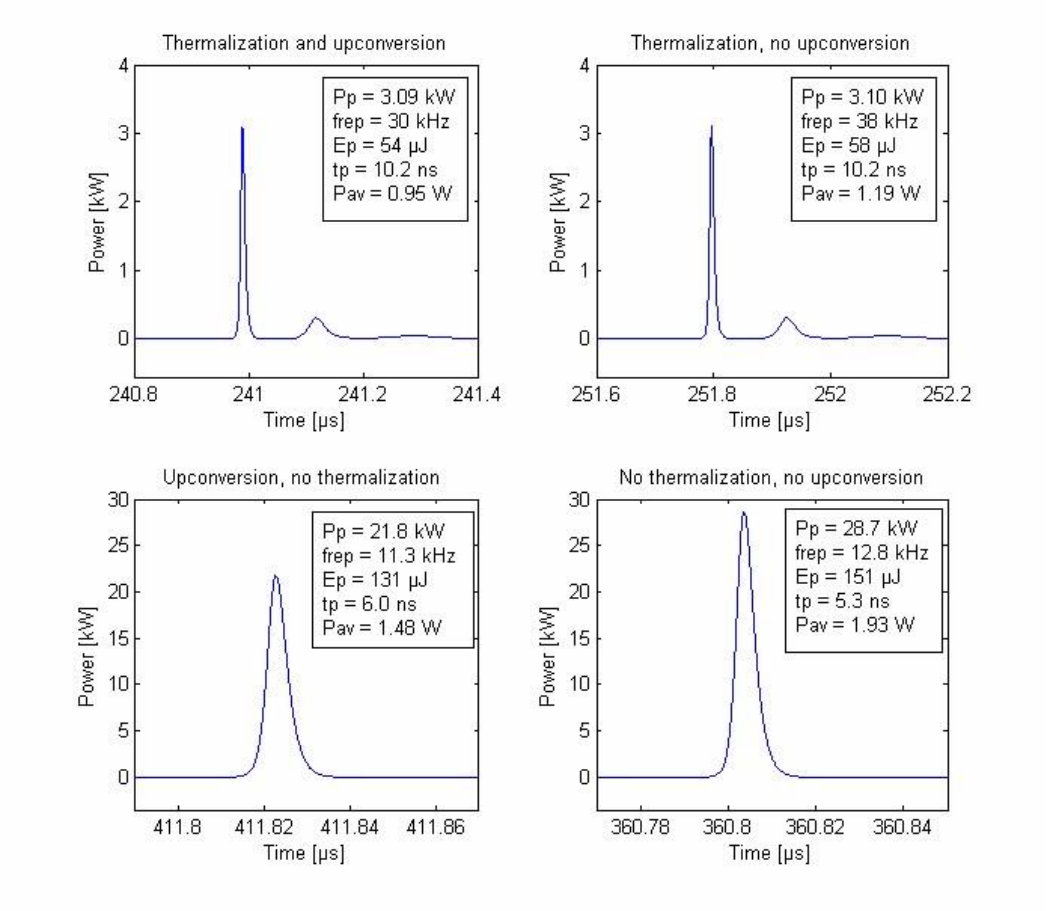

Fig. 2.5 Pulse characteristics with and without thermalization and upconversion.

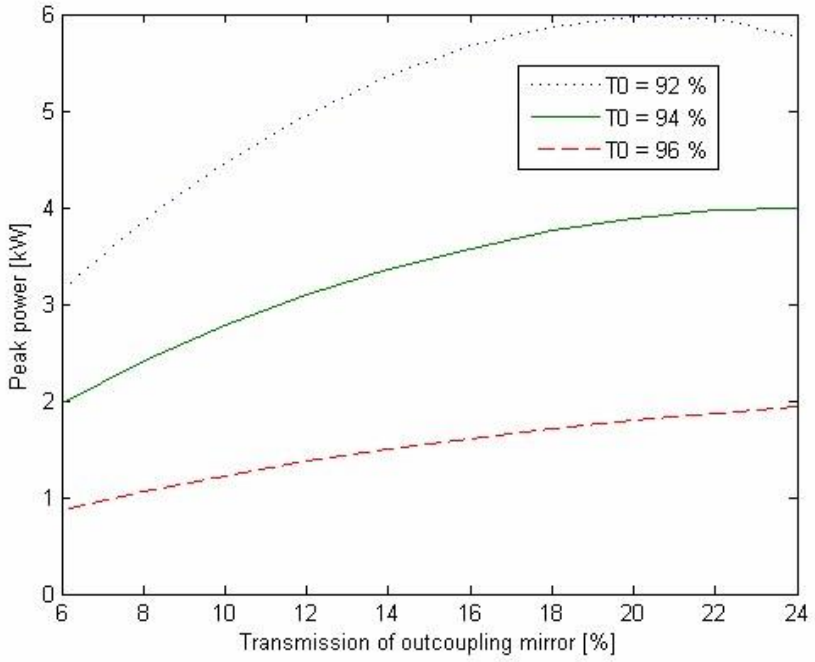

Fig. 2.6 The peak power as function of transmission of outcoupling mirror for different values of the initial transmission of the Cr:YAG crystal.

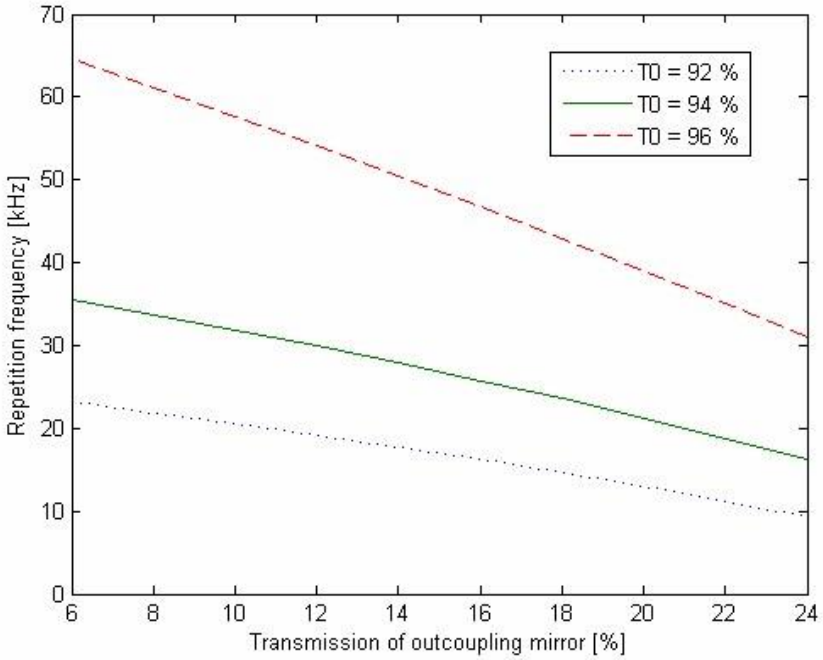

Fig. 2.7 The repetition frequency as function of transmission of outcoupling mirror for different values of the initial transmission of the Cr:YAG crystal.

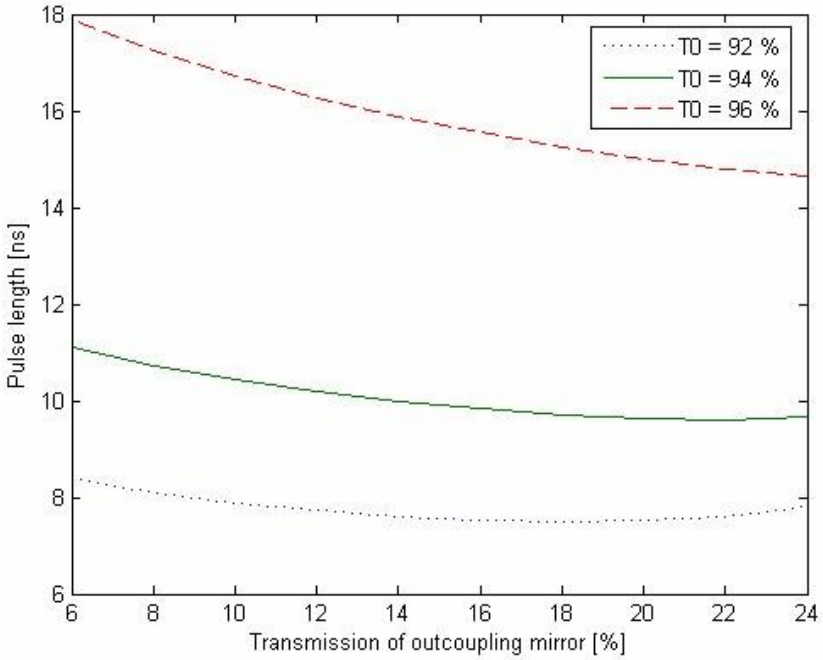

Fig. 2.8 The pulse length as function of transmission of outcoupling mirror for different values of the initial transmission of the Cr:YAG crystal.

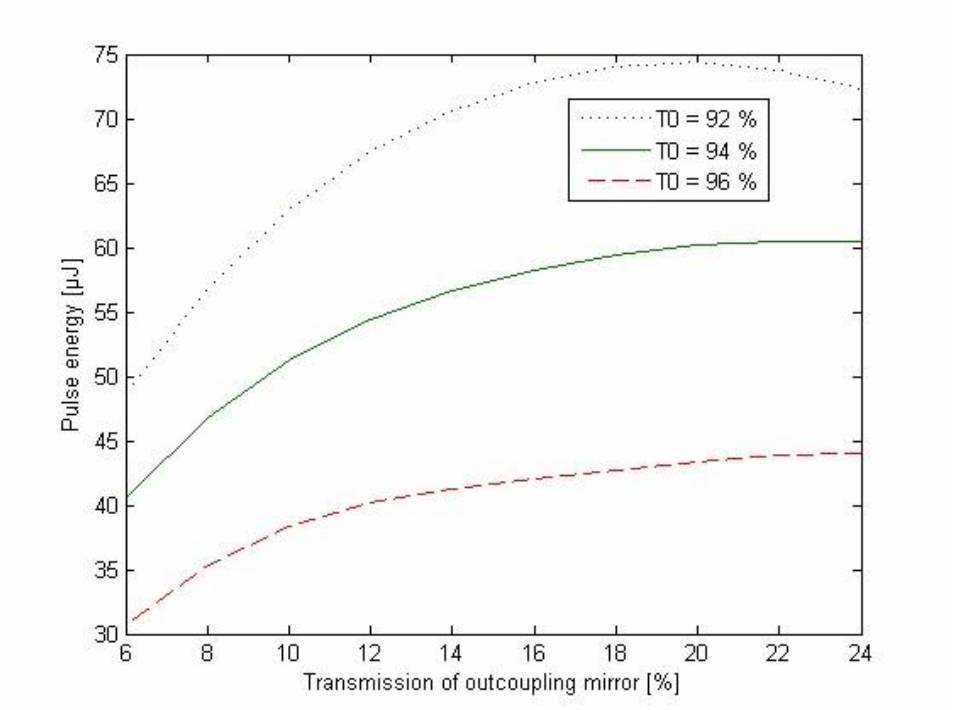

Fig. 2.9 The pulse energy as function of transmission of outcoupling mirror for different values of the initial transmission of the Cr:YAG crystal.

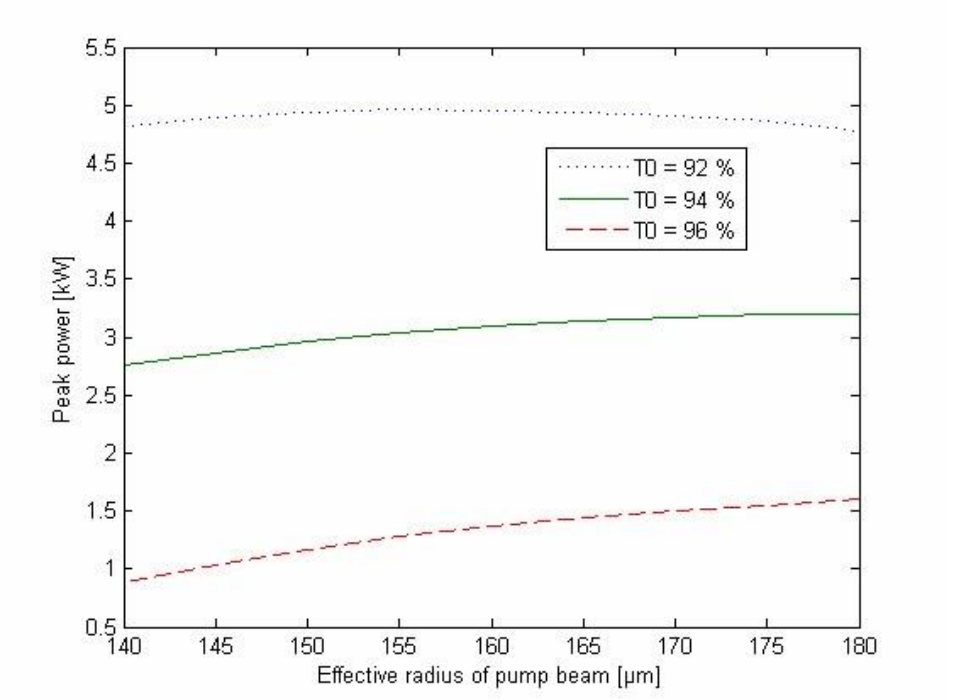

Fig. 2.10 The peak power as function of the effective radius of the pump beam for different values of the initial transmission of the Cr:YAG crystal.

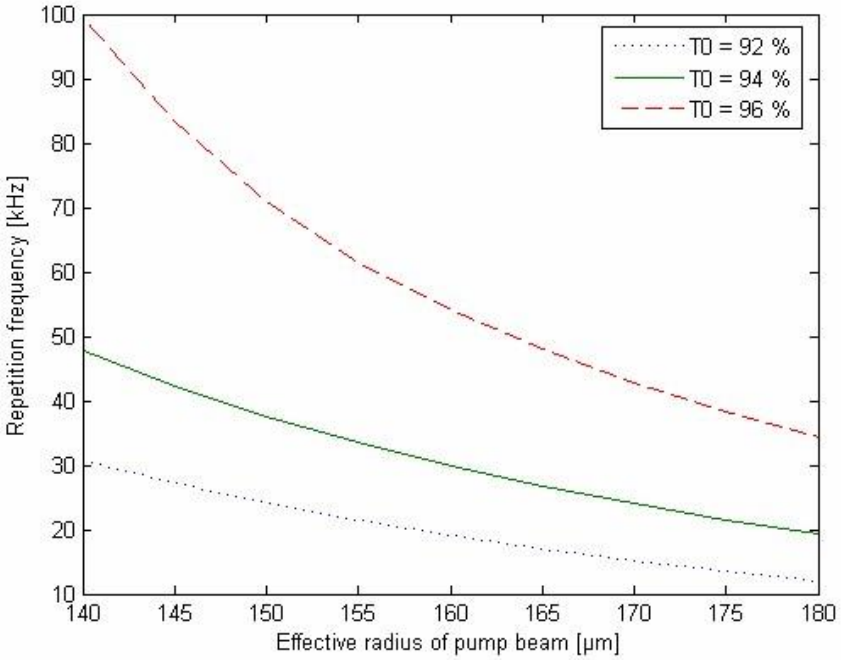

Fig. 2.11 The repetition frequency as function of the effective radius of the pump beam for different values of the initial transmission of the Cr:YAG crystal.

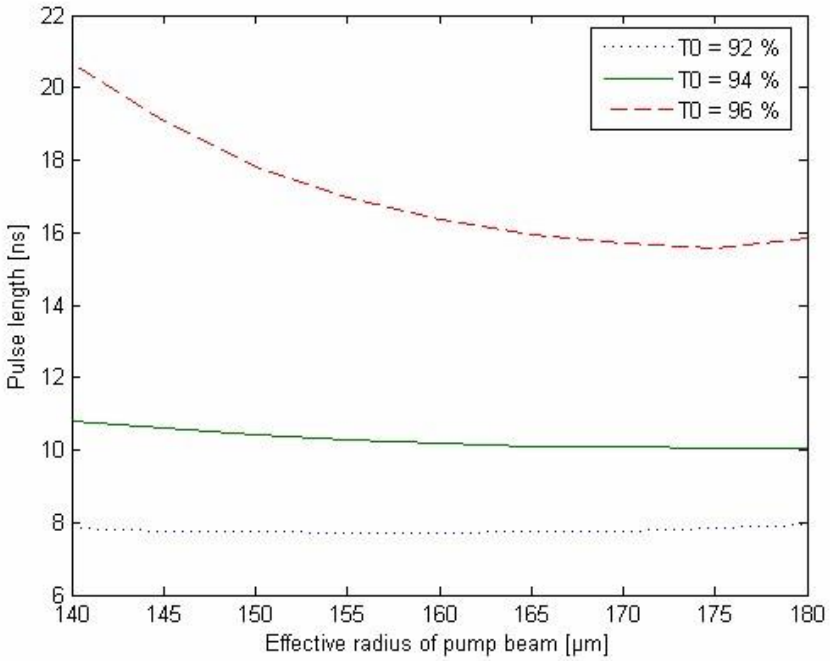

Fig. 2.12 The pulse length as function of the effective radius of the pump beam for different values of the initial transmission of the Cr:YAG crystal.

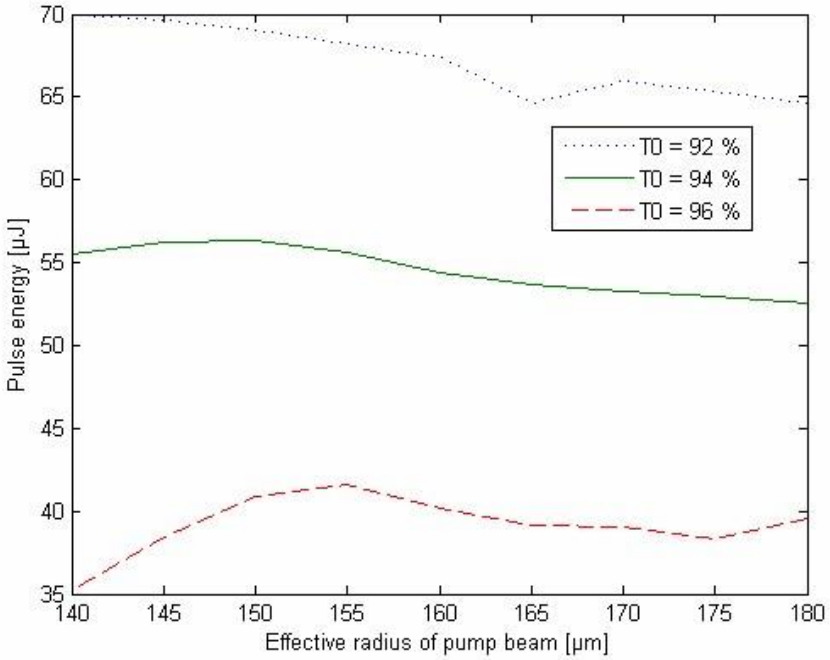

Fig. 2.13 The pulse energy as function of the effective radius of the pump beam for different values of the initial transmission of the Cr:YAG crystal.